

MIT Open Access Articles

Beam steering via peak power decay in nonlinear waveguide arrays

The MIT Faculty has made this article openly available. **Please share** how this access benefits you. Your story matters.

Citation: Droulias, Sotiris, Yoav Lahini, Yannis Kominis, Panagiotis Papagiannis, Yaron Bromberg, Kyriakos Hizanidis, and Yaron Silberberg. "Beam steering via peak power decay in nonlinear waveguide arrays." *New Journal of Physics* 15, no. 9 (September 1, 2013): 093038.

As Published: <http://dx.doi.org/10.1088/1367-2630/15/9/093038>

Publisher: IOP Publishing

Persistent URL: <http://hdl.handle.net/1721.1/83196>

Version: Final published version: final published article, as it appeared in a journal, conference proceedings, or other formally published context



Beam steering via peak power decay in nonlinear waveguide arrays

This content has been downloaded from IOPscience. Please scroll down to see the full text.

2013 New J. Phys. 15 093038

(<http://iopscience.iop.org/1367-2630/15/9/093038>)

View [the table of contents for this issue](#), or go to the [journal homepage](#) for more

Download details:

IP Address: 18.51.1.88

This content was downloaded on 09/12/2013 at 15:59

Please note that [terms and conditions apply](#).

Beam steering via peak power decay in nonlinear waveguide arrays

Sotiris Droulias^{1,5,6}, Yoav Lahini², Yannis Kominis^{1,3},
Panagiotis Papagiannis¹, Yaron Bromberg⁴, Kyriakos Hizanidis¹
and Yaron Silberberg⁴

¹ School of Electrical and Computer Engineering, National Technical University of Athens, Athens 15773, Greece

² Department of Physics, Massachusetts Institute of Technology, Cambridge, MA 02139, USA

³ Department of Mathematics, University of Patras, Patras 26500, Greece

⁴ Department of Physics of Complex Systems, the Weizmann Institute of Science, 76100 Rehovot, Israel

E-mail: sdroulias@iesl.forth.gr

New Journal of Physics **15** (2013) 093038 (14pp)

Received 21 May 2013

Published 25 September 2013

Online at <http://www.njp.org/>

doi:10.1088/1367-2630/15/9/093038

Abstract. We report the experimental observation and theoretical analysis of a novel beam-steering effect in periodic waveguide arrays that arises from the interplay between discrete diffraction, Kerr nonlinearity and any mechanism that effectively weakens the nonlinear part of the beam. In this regime the propagation direction shows increased sensitivity to the input angle and for a certain angular range around normal incidence a nonlinear beam may be guided to a direction opposite to that initially inserted. For continuous wave beams the role of this mechanism is played by absorption of any kind, such as three photon absorption, two photon absorption or even linear absorption. For pulsed beams we show that the same dynamics can arise due to strong normal temporal dispersion, while absorption is not necessary and can be a further enhancing

⁵ Current affiliation: Institute of Electronic Structure and Laser, FORTH, 71110 Heraklion, Crete, Greece.

⁶ Author to whom any correspondence should be addressed.



Content from this work may be used under the terms of the [Creative Commons Attribution 3.0 licence](https://creativecommons.org/licenses/by/3.0/). Any further distribution of this work must maintain attribution to the author(s) and the title of the work, journal citation and DOI.

or alternative factor. This observation falls under a more general dissipation-assisted beam velocity control mechanism in nonlinear optical lattices, which is also theoretically predicted by the effective particle approach.

Contents

1. Introduction	2
2. Experimental results	3
3. Continuous wave (CW) systems: the effective particle approach	5
4. CW systems: simulations	7
5. Extension to CW systems with linear absorption or two photon absorption	10
6. Pulsed systems	11
7. Conclusions	13
Acknowledgments	13
References	13

1. Introduction

Nonlinear optical waveguide lattices have been intensely studied in the past few years, revealing a wealth of properties that are not encountered in homogeneous media [1]. It is now well established that this is mainly due to their structural periodicity that may significantly alter their diffraction properties, a fact that is reflected in both the linear and nonlinear regime. For example, tailored diffraction properties of optical wave fronts [2] are possible in the linear domain whereas discrete optical solitons can form under nonlinear conditions [3], just to mention a few striking phenomena. It is the unique characteristics of these configurations that render them an effective medium for controlling the propagation of light.

So far, several schemes toward this direction have theoretically been proposed and experimentally realized. In the linear regime, the idea of applying a linearly varying potential in the transverse direction so as to produce photonic Bloch oscillations [4, 5] has been utilized in thermo-optic waveguide arrays [6], where the beam velocity is controlled by the transverse temperature gradient. In another implementation the varying potential is achieved by a linearly growing effective index of the individual guides [7]. Quite recently discrete beam acceleration, a different concept based on the propagation of non-diffractive, self-bending Airy beams in bulk homogeneous media [8], has been theoretically demonstrated in uniform optical lattices [9]. In the nonlinear regime, power-controlled beam steering may be achieved with linearly chirped or unchirped [10, 11] solitons. The beam output position may be also controlled by an either externally or internally induced velocity [12, 13], the latter stemming from an input beam shift relative to the waveguides. Moreover, array inhomogeneity [14], engineered defects or a superimposed linear guided mode [15], as well as interaction with a continuous wave (CW) background [16] may induce controllable soliton steering.

In all these cases absorption was considered absent or negligible in both experiments and theoretical analysis for the configurations examined, as it was always assumed it can only degrade or even inhibit beam steering. If another competitive mechanism, such as optical gain is present whenever absorption is countable, dissipative soliton formation is possible [17] and beam velocity control is maintained [18]. Nevertheless, even in the absence of a power

restoring mechanism, non-negligible absorption may lead to an interesting dynamical behavior of a focused beam [19].

Moreover, in the cases mentioned above, the interest has been focused on the spatial behavior of light, rather than its temporal evolution, by either considering CW beams or measuring time-integrated pulses at the system output. Only recently it was shown that a pulsed beam propagating in a discrete system may lead to interesting patterns, such as discrete X-waves [20], which cannot be otherwise observed if the temporal dimension is either ignored or absent.

Within this framework, in this work we observe experimentally and study numerically the spatiotemporal beam dynamics in periodic lattices and show how the temporal evolution may have a direct implication in the spatial propagation direction of light. Although the dynamics may be complex, we propose a simple concept of how to control the beam's direction in a predictable non-chaotic manner. To clarify the underlying mechanism we begin with the study of a CW system with three photon absorption (3PA) and theoretically show how absorption acts as a longitudinally dynamical potential variation. For the sake of generality we also explain why the same dynamics are feasible in similar systems that exhibit any relative kind of absorption, such as two photon absorption (2PA) or even linear absorption. Next, we extend the conclusions to pulsed systems and show how this potential variation is now induced by the spatiotemporal dynamics, rather than an absorptive mechanism, the presence of which is enhancing but not necessary. Our calculations and predictions are in good agreement with experiments performed in an AlGaAs waveguide array system.

2. Experimental results

The system under investigation is a 5 mm long waveguide array, fabricated in an AlGaAs planar waveguide by way of conventional photolithography techniques. The waveguides are $4\ \mu\text{m}$ wide, and the array period is $D = 8.5\ \mu\text{m}$. The areas between waveguides exhibit a low refractive index (RI) of $n_0 = 3.3244$, while the lateral effective RI step is $\Delta n = 0.0011$. This relatively small value that stems from the shallow etching depth, results in a strong coupling constant of $950\ \text{m}^{-1}$ between waveguides. The laser beam that enters the sample operates at 1530 nm and the self-focusing Kerr coefficient is $\hat{n}_2 = 1.5 \times 10^{-13}\ \text{cm}^2\ \text{W}^{-1}$. Although 2PA is negligible, 3PA is present, yielding a coefficient $\alpha_3 = 10^{-4}\ \text{m}^{-1}\ \text{W}^{-2}$. The dispersion in the AlGaAs array is approximately $\beta_2 = 1.35\ \text{ps}^2\ \text{m}^{-1}$. The experimental setup is shown in figure 1.

Our laser source is an optical parametric oscillator (Spectra-Physics OPAL), pumped by a 810 nm Ti:sapphire (Tsunami) laser, producing 170 fs pulses at a repetition rate of 80 MHz at a wavelength of 1530 nm. The input power to the sample is adjusted by a variable filter. A cylindrical lens at the back focal plane of the $40\times$ input objective was used to shape the input beam. Shifts of the beam's axis before the input objective was used to induce a linear phase chirp to the beam at the input facet of the array, thus controlling the initial propagation angle in the array. Light is coupled into the waveguide array, propagates in it and is collected from the output facet, to be imaged using a CCD camera.

In order to scan the beam output position in terms of the input transverse velocity, the beam is tilted within a range of at least -13.5 and 13.5 mrad, which for the specific system covers the $(-\pi/2, \pi/2)$ range of the transverse Bloch momentum $Q = k_x D$. In this configuration, a Gaussian beam of $12\ \mu\text{m}$ full-width half-maximum (FWHM) input spatial extent is used, which covers approximately 2–3 waveguides. The scan starts at low power levels and is repeated with

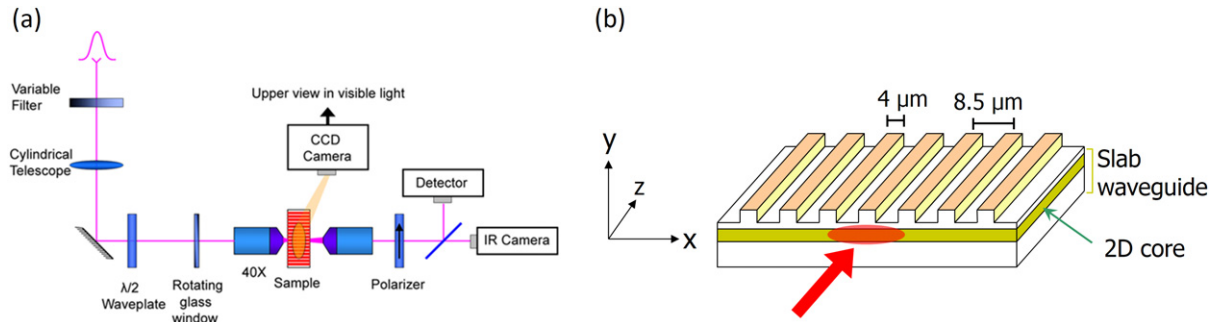


Figure 1. (a) Experimental setup and (b) schematic view of the sample and the coupling geometry.

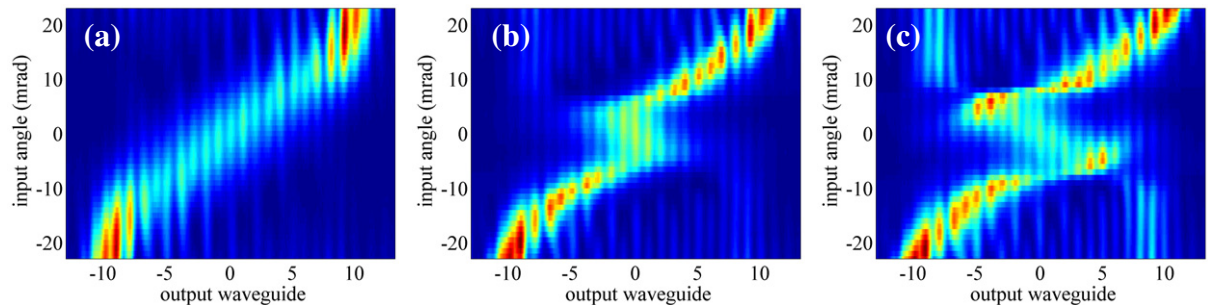


Figure 2. Experimental observation of the output beam position versus input beam angle for propagation of a 170 fs sech-type 12 μm FWHM Gaussian beam, initially placed on the central waveguide. At low input peak power (a) the propagation is linear, while for high peak power (625 W) the wiggly pattern starts to form (b) until it becomes prominent at 875 W (c). For each input angle the output is taken at $z = 5$ mm and integrated in time.

higher power beams. This procedure is carried out twice, with respect to the input position of the beam's peak. The first time it overlaps with the midpoint of the central waveguide and in the second case it is positioned between the central and the adjacent waveguide.

The experimental output beam position versus the input beam tilt for both scans is presented in figures 2 and 3, for low as well as high power pulsed beams. In these figures, the beam output for every scanned input angle is taken at the sample exit ($z = 5$ mm) and integrated in time. The horizontal axis is always normalized to the array period D , unless stated otherwise.

At low input power levels, as light propagates in the sample, it couples to adjacent waveguides and undergoes discrete diffraction. When the beam deviates from normal incidence, the wave front is directed according to the curvature of the diffraction diagram, essentially following up the input tilt as theoretically expected. Hence, during linear propagation the output position versus input beam tilt pattern follows the familiar cosine-like behavior, which reflects the first band curvature of the periodic system [2] (see e.g. figures 2(a) and 3(a)). However, at high input power levels where the beam propagates in a nonlinear fashion, the output pattern can be significantly altered, depending on the initial beam peak position. For a certain angular range around normal incidence the beam is guided to a direction opposite to that initially inserted when the beam is centered on the central waveguide (figure 2), behavior that does not take place

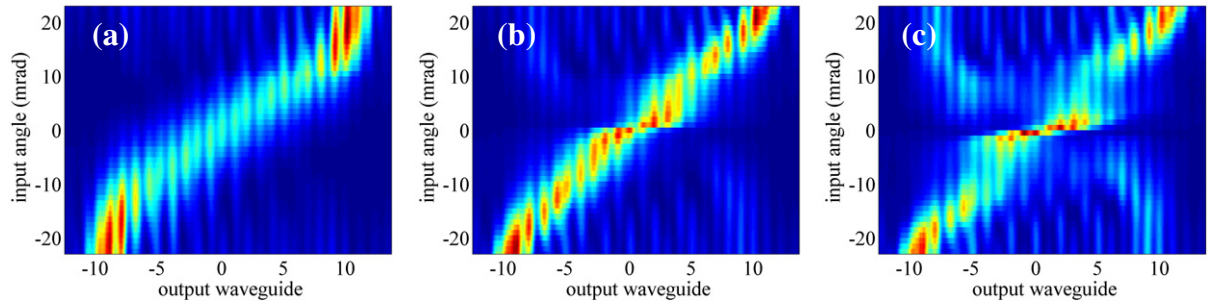


Figure 3. Experimental observation of the output beam position versus input beam angle for propagation of a 170 fs sech-type 12 μm FWHM Gaussian beam, initially placed between the central and the adjacent waveguide. At low input peak power (a) the propagation is linear, while as the peak power is increased no wiggly pattern appears (625 W in (b) and 875 W in (c)). For each input angle the output is taken at $z = 5$ mm and integrated in time.

when the beam is positioned between waveguides (figure 3). Typically, a narrow beam at such high power levels would be expected to form a discrete soliton in the input waveguide for a certain angular range around normal incidence [13], fact that raises the question of how this counter-intuitive behavior takes place.

3. Continuous wave (CW) systems: the effective particle approach

To gain insight into the complex beam dynamics, let us first begin with a pertinent CW system. In this case beam propagation is described by a modified nonlinear Schrödinger (NLS) equation, which includes the transverse variation of the RI. In its general form with the appropriate absorption terms added, the equation reads

$$i \frac{\partial u}{\partial z} + \frac{1}{2k_0 n_0} \frac{\partial^2 u}{\partial x^2} + k_0 \Delta n(x) u + k_0 \hat{n}_2 |u|^2 u + i (\alpha_1 + \alpha_2 |u|^2 + \alpha_3 |u|^4) u = 0, \quad (1)$$

where $k_0 = 2\pi/\lambda_0$ is the free-space wavenumber, $\Delta n(x)$ the RI modulation and n_0 the lowest value of the RI. \hat{n}_2 is the nonlinear Kerr coefficient and β_2 the group velocity dispersion (GVD) term, while α_1 , α_2 and α_3 are the linear absorption, 2PA and 3PA coefficients, respectively.

To stress the generality of the dynamics, let us normalize equation (1) with a simple coordinate transformation, i.e. $\zeta = z/Z_0$, $\chi = x/X_0$ and $U = u/U_0$. Under this normalization equation (1) is written as

$$i \frac{\partial U}{\partial \zeta} + \frac{\partial^2 U}{\partial \chi^2} + 2|U|^2 U = n(\chi) U - i (\sigma_1 + \sigma_2 |U|^2 + \sigma_3 |U|^4) U, \quad (2)$$

with $n(\chi) = -2n_0 k_0^2 X_0^2 \Delta n(X_0 \chi)$, $\sigma_1 = Z_0 \alpha_1$, $\sigma_2 = Z_0 U_0^2 \alpha_2$, $\sigma_3 = Z_0 U_0^4 \alpha_3$, where

$$Z_0 = 2k_0 n_0 X_0^2 \quad \text{and} \quad U_0^2 = \frac{1}{k_0^2 n_0 \hat{n}_2 X_0^2}. \quad (3)$$

Equation (2) with zero rhs corresponds to the integrable NLS equation with the soliton solution $U = \eta \operatorname{sech}[\eta(\chi - \chi_0)] \exp[i(v\chi/2 + 2\phi)]$. η is the amplitude or the inverse width

of the soliton solution, χ_0 is the position of its center (called sometimes the center of mass due to the effective-particle analogy of the solitons), v is the transverse velocity and ϕ is the nonlinear phase shift. If we consider a relatively shallow lattice with low absorption, for which equation (2) is allowed to be treated via a perturbative approach, then the soliton can be treated as an effective particle [21] of variable mass $m = \int |U|^2 d\chi = 2\eta$ and momentum $p = mv$ at a position χ_0 moving in an effective potential due to the lattice according to the equations

$$\frac{dm}{d\zeta} = -2m \left(\sigma_1 + \frac{\sigma_2}{6} m^2 + \frac{\sigma_3}{30} m^4 \right), \quad (4)$$

$$\frac{dp}{d\zeta} = -\frac{\partial V_{\text{eff}}}{\partial \chi_0} \quad \text{and} \quad \frac{d\chi_0}{d\zeta} = \frac{p}{m}. \quad (5)$$

Let us for simplicity consider a sinusoidal RI modulation, varying as $n(\chi) = A \sin(K\chi)$, for which the effective potential is simply calculated as

$$V_{\text{eff}} = \frac{2A\pi K}{\sinh(\pi K/m)} \sin(K\chi_0). \quad (6)$$

In the absence of absorption ($\sigma_1 = \sigma_2 = \sigma_3 = 0$) the effective particle motion described by equations (4) and (5) is integrable and stationary stable and unstable solitons are formed in the minima and the maxima of the effective potential, respectively. Moreover, two distinct dynamical behaviors are described, one corresponding to trapped solitons oscillating around a potential minimum and the other to traveling solitons moving transversely across the potential, depending on the initial energy of the effective particle. A soliton initially located at the minimum of the potential can be untrapped only if its initial velocity exceeds a critical value

$$v_{\text{cr}} = 2 \left(\frac{2A\pi K/m}{\sinh(\pi K/m)} \right)^{1/2}. \quad (7)$$

From equations (6) and (7) it is obvious that in the same periodic medium solitons of different mass move in effective potentials of different strength and consequently different critical velocities. In fact, it is apparent from equation (7) that solitons of higher mass require higher velocities to escape their periodic orbit, which is trapped within the potential minimum they are launched, in other words they experience a stronger effective potential.

In the presence of absorption ($\sigma_1, \sigma_2, \sigma_3$ or their combination) the soliton mass reduces according to equation (4) until it essentially settles down after a transient propagation distance where the nonlinear effects are relaxed due to mass reduction. Consequently, via this procedure absorption is translated into a dynamical modulation (weakening) of the effective potential V_{eff} . If the soliton is initially launched at a potential minimum with $v < v_{\text{cr}}$ it starts to oscillate within this minimum, until its mass has been reduced enough so that it may escape. Depending on the propagation distance at which this happens, the output angle may follow a complex pattern, since this can occur at any random moment of the oscillatory motion. If, however, absorption is such that the escape can occur within the first half-period of oscillation, then an interesting and predictable pattern emerges, as depicted in the example of figure 4(a) for a system with 3PA ($\sigma_1 = \sigma_2 = 0, \sigma_3 \neq 0$).

For small initial velocities the soliton escapes the periodic motion within the first half-cycle of oscillation at a direction opposite to that initially launched. For larger initial velocities, the soliton directly escapes the input minimum (within the first quarter cycle of oscillation)

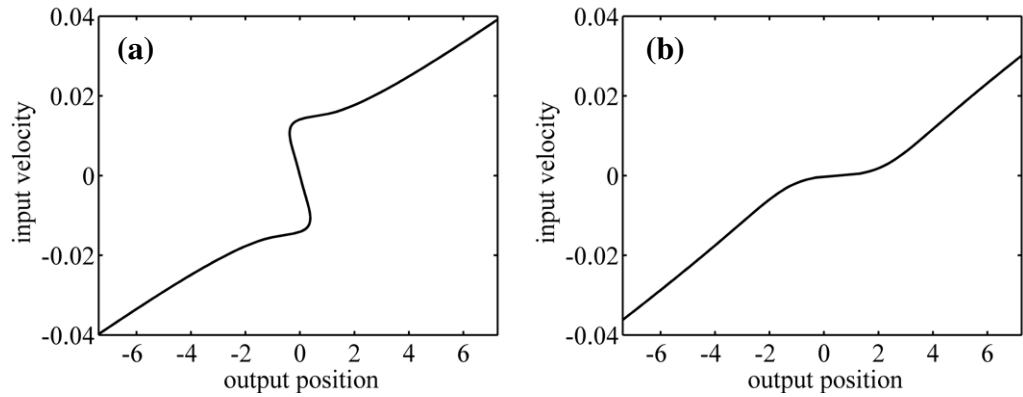


Figure 4. Input velocity versus output soliton center position measured at $\zeta = 1000$ for a system with $A = 10^{-2}$, $K = 1$ and $\sigma_3 = 0.5$. A soliton of initial mass $m_o = 0.4$ is launched at (a) potential minimum $\chi_o = -\pi/2K$ and (b) potential maximum $\chi_o = \pi/2K$. The x -axis is shifted $\pi/2K$ units to the left and normalized to the period $2\pi/K$ of the RI modulation, so that the output position ticks mark the potential minima.

following a trajectory more or less along the initial angle, giving birth to this wiggly pattern. On the other hand, a soliton launched at a potential maximum is unstable and even the slightest initial velocity is sufficient to repel it from its input position, thus approximately following the input direction, as figure 4(b) implies. Similar patterns arise when considering $\sigma_2 \neq 0$ or $\sigma_1 \neq 0$ and this behavior falls under a more general case for dissipative optical lattices, which has been analyzed in detail in our previous work [18].

4. CW systems: simulations

Let us now consider a system with stronger lattice modulation and 3PA, similar to the scenario realized in our experiment. Although the experiment was carried out with 170 fs pulses, let us in this section assume a hypothetical experiment with a CW beam, where only discrete diffraction, Kerr nonlinearity and 3PA are present (no thermal or other effects are considered).

To simulate the results numerically, the coefficients of equation (1) as well as the input beam parameters are set to the values used in our experiment. The temporal term has been removed and $\alpha_1 = \alpha_2 = 0$ has been considered. To make the role of absorption clearer, in these CW simulations 3PA has been set to $\alpha_3 = 7 \times 10^{-4} \text{ m}^{-1} \text{ W}^{-2}$, i.e. seven times higher than the real value. The output beam position versus the input beam tilt of the hypothetical experiment and the respective simulations is presented in figure 5 for low as well as high power beams.

It is worth mentioning that, in contrast to the scenario analyzed with the effective particle approach, here not only the lattice exhibits strong RI modulation and strong 3PA, but also the beam is spatially Gaussian and not sech-like, yet, the two systems retain similar properties.

The key to understanding this resemblance lies in the stability of the initial state that is excited in each case. In case the beam peak is placed on the central waveguide this position corresponds to a potential minimum of the former theoretical analysis. When the input power is increased, the initially narrow Gaussian beam undergoes self-focusing and is ‘locked’ within the same waveguide, forming a discrete soliton. Under an initial tilt, if no absorption mechanism

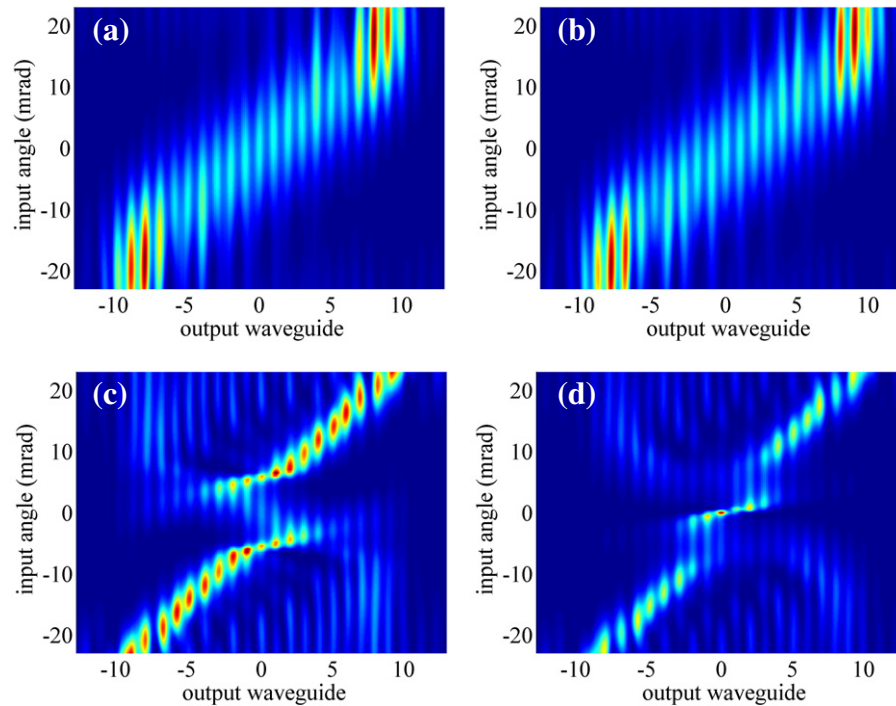


Figure 5. Simulations of the output beam position versus input beam angle for a hypothetical experiment with a CW Gaussian beam of $12\ \mu\text{m}$ FWHM. Beam center initially placed on the central waveguide (a, c) and between the central and the adjacent waveguide (b, d). At low input power (a, b) the propagation is linear, while for nonlinear propagation at 875 W peak power (c, d) the wiggly pattern forms only when the input beam is placed on the central waveguide (c). For each input angle the output is taken at $z = 5\ \text{mm}$.

is present, the self-trapped beam starts to oscillate within the waveguide. The presence of 3PA intervenes in the oscillatory motion, exactly as explained with the effective particle approach and is depicted in figure 6 for the system in hand, where it is demonstrated how the distance, at which the beam escapes, approaches $z = 0$ as absorption increases. Finally, for further tilt, the oscillation amplitude becomes greater (while the period shortens) until the beam escapes, approximately following the input angle.

Since the optical power diminishes, the beam eventually propagates in a linear manner, thus discretely diffracting toward the new direction. In this procedure, side radiation acts as a further power damping factor for the initially localized state (see figure 6(a) for example), thus facilitating beam delocalization.

Interestingly, when 3PA is very intense, regardless of the input tilt the beam peak is very quickly damped, and the output beam trace resembles that of linear propagation since the mass-dependent effective potential drastically reduces. On the other hand, when 3PA is rather small, then the intense nonlinearity combined with discrete diffraction may lead to complex patterns. Both scenarios are presented in figure 7.

In case the input beam peak is placed between two waveguides, position corresponding to a potential maximum, the excited nonlinear state is unstable [22]. A slight transverse velocity, inaccurate displacement or even material imperfection will push the beam to the

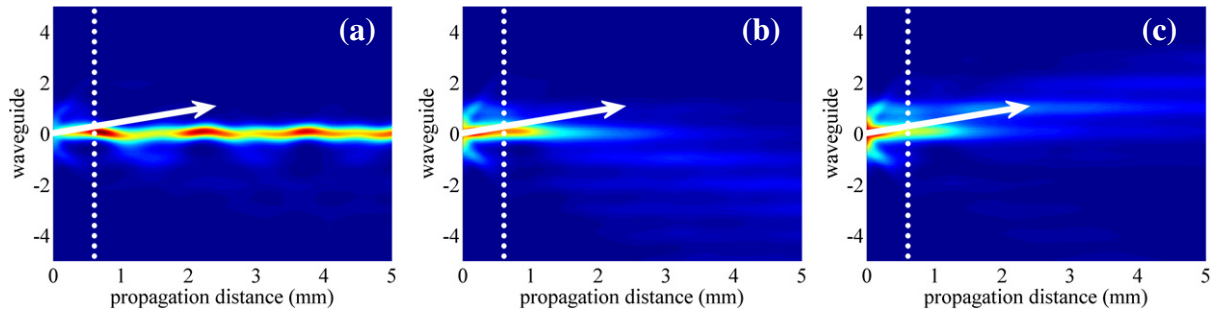


Figure 6. Explicit evolution of the CW beam presented in figure 5(c) at an input angle of 4 mrad. (a) In the absence of absorption the beam is strongly localized due to the intense nonlinearity and oscillates within the central waveguide. (b) The same beam under 3PA ($\alpha_3 = 7 \times 10^{-4} \text{ m}^{-1} \text{ W}^{-2}$) escapes the central waveguide in a direction opposite to the input before the 1st half-period of oscillation. (c) The same beam under stronger 3PA (three times that of (b)) is released before the first quarter period of oscillation and consequently in the same direction. In all cases the white arrow indicates the direction of initial tilt and the dotted line marks the propagation distance of first quarter period of oscillation.

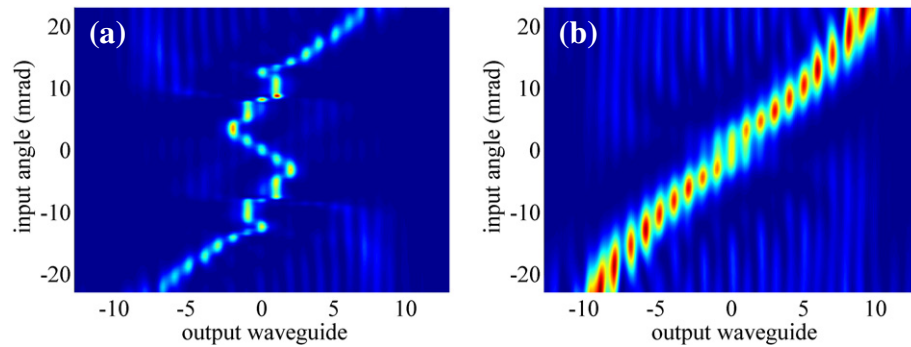


Figure 7. Simulations of the output beam position versus input beam angle for nonlinear propagation of a $12 \mu\text{m}$ FWHM Gaussian CW beam at peak power of 875 W with input beam peak coupled to the central waveguide. (a) Complex pattern for low 3PA ($\alpha_3 = 1 \times 10^{-4} \text{ m}^{-1} \text{ W}^{-2}$). (b) Pattern resembling linear propagation for intense 3PA ($\alpha_3 = 30 \times 10^{-4} \text{ m}^{-1} \text{ W}^{-2}$). For each input angle the output is taken at $z = 5 \text{ mm}$.

nearest waveguide, while undergoing an uneven power splitting among the two adjacent sites. Inevitably, the small part of the beam that remains on one waveguide weakens the major beam part that jumps on the other and starts oscillating, while being further deteriorated by side radiation. Hence, even at small angles the beam is less prone to trapping and consequently lower absorption levels are capable of making such a phenomenon possible. This is why for the 3PA level of the given sample such a pattern is not observed, as already demonstrated in figure 5(d).

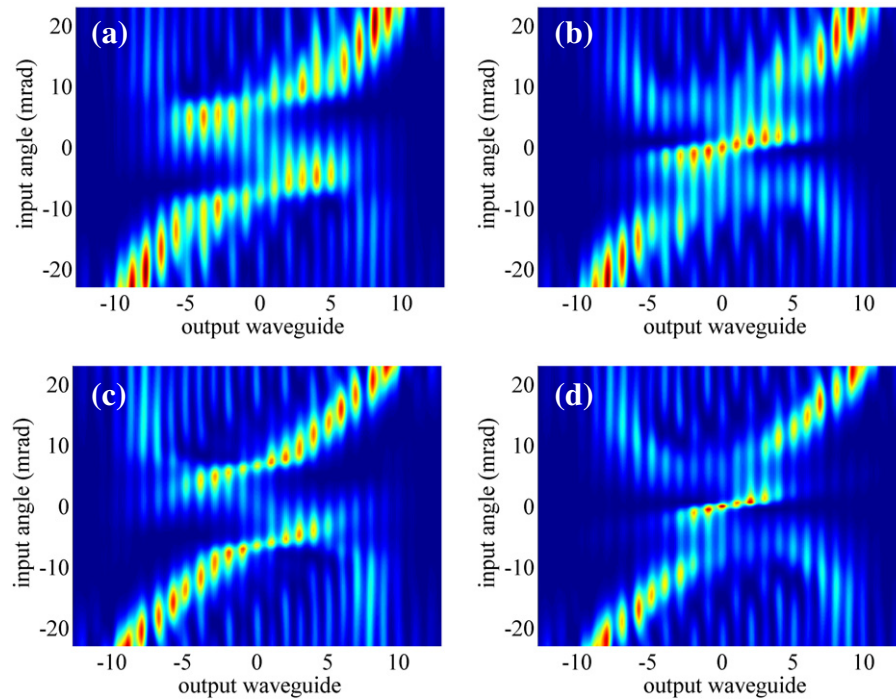


Figure 8. Output beam position versus input beam angle for nonlinear propagation at peak power of a $12\ \mu\text{m}$ FWHM Gaussian CW beam at peak power of 875 W with input beam peak coupled to the central waveguide in (a, c) and between adjacent waveguides in (b, d). Simulation of the same as in experiment hypothetical structure, which instead of 3PA exhibits (a, b) linear absorption with $\alpha_1 = 370\ \text{m}^{-1}$ or (c, d) 2PA with $\alpha_2 = 0.5\ \text{m}^{-1}\ \text{W}^{-1}$. For each input angle the output is taken at $z = 5\ \text{mm}$.

5. Extension to CW systems with linear absorption or two photon absorption

From the preceding analysis it is apparent that in the CW case the key to this extraordinary effect is the presence of an absorptive mechanism that acts effectively within the first half-cycle of beam oscillation in its initial confinement. To demonstrate how this can also be accomplished by any kind of relative absorption we set $\alpha_3 = 0$ in equation (1) and assume the linear absorption and 2PA coefficients to be $\alpha_1 = 370\ \text{m}^{-1}$ and $\alpha_2 = 0.5\ \text{m}^{-1}\ \text{W}^{-1}$, respectively. Successively switching them on, the simulations for a hypothetical system of the exact same parameters, which instead of 3PA exhibits either linear absorption or 2PA, are presented in figure 8.

As expected, the simulations reveal a performance similar to that of figures 5(c) and (d). The main difference lies in the propagating distance along which each kind of absorption acts. Since 3PA acts proportionally to $\sim |u|^4$, it switches off sooner than the respective system with 2PA ($\sim |u|^2$) or with linear absorption, where optical power constantly deteriorates. Consequently, in terms of power consumption, a system with 3PA would be considered more advantageous. As already mentioned, similar patterns are also predicted by the effective particle approach when considering $\sigma_2 \neq 0$ or $\sigma_1 \neq 0$ and hence this counter-intuitive effect of the dissipative mechanisms is simply explained.

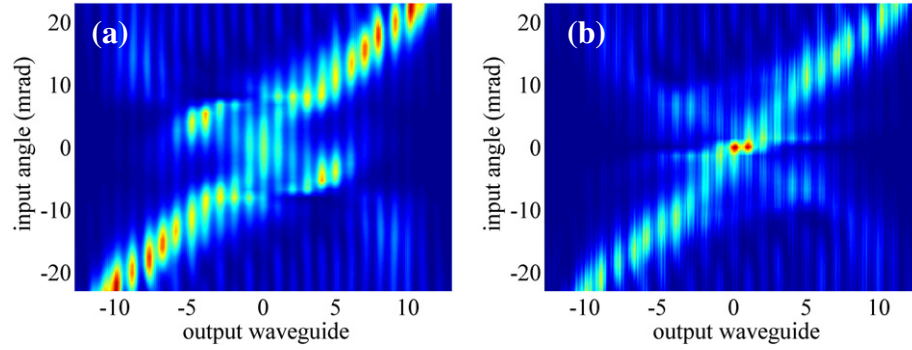


Figure 9. Simulations of the output beam position versus input beam angle for propagation of a 170 fs sech-type 12 μm FWHM Gaussian beam of 875 W input peak power. Beam initially placed (a) on the central waveguide and (b) between the central and the adjacent waveguide. For each input angle the output is taken at $z = 5$ mm and integrated in time. These results are in agreement with the experiments (compare to figures 2(c) and 3(c)).

6. Pulsed systems

Thus far it has been evident that the excitation of a pattern similar to the one observed in the experiments requires the presence of a mechanism that is able to weaken the nonlinear part of the beam, i.e. the beam peak power, in an effective way. Returning to our experimental situation, it can now be simply explained why in the case of pulses this can be directly provided by any process leading to pulse broadening, such as the combined effect of normal dispersion with Kerr nonlinearity.

The output pattern depends on the beam's peak input position as explained in the CW case. The dynamical potential variation is now realized by the combined action of normal dispersion and discrete diffraction in the presence of Kerr nonlinearity. As the pulse propagates, the nonlinear main part of the pulse behaves in the oscillatory fashion described previously, while the weak edges undergo discrete diffraction. Due to the high normal dispersion of AlGaAs and the presence of Kerr nonlinearity the pulse is also subject to severe broadening. Consequently, the pulse broadening, which leads to peak power decrease, weakens the initially strongly nonlinear main part of the pulse, intervening in the oscillatory motion in a fashion similar to that of absorption in a CW system.

To simulate the pulsed beam propagation numerically we have included the appropriate temporal term in equation (1), which for $\alpha_1 = \alpha_2 = 0$ now reads

$$i \frac{\partial u}{\partial z} + \frac{1}{2k_0 n_0} \frac{\partial^2 u}{\partial x^2} - \frac{\beta_2}{2} \frac{\partial^2 u}{\partial t^2} + k_0 \Delta n(x) u + k_0 \hat{n}_2 |u|^2 u + i\alpha_3 |u|^4 u = 0. \quad (8)$$

The simulated output beam position versus the input beam tilt for high input peak power of 875 W is presented in figure 9. Here, the beam output for every scanned input angle is taken at the sample exit ($z = 5$ mm) and integrated in time, exactly as in experimental figures 2 and 3. Figures 9(a) and (b) correspond to figures 2(c) and 3(c), respectively. In all cases, the numerical simulations are in excellent agreement with the experimental data.

To better illustrate the essence of this mechanism, in figure 10 we present the full spatiotemporal profile of the simulated pulse together with the time-integrated spatial profile.

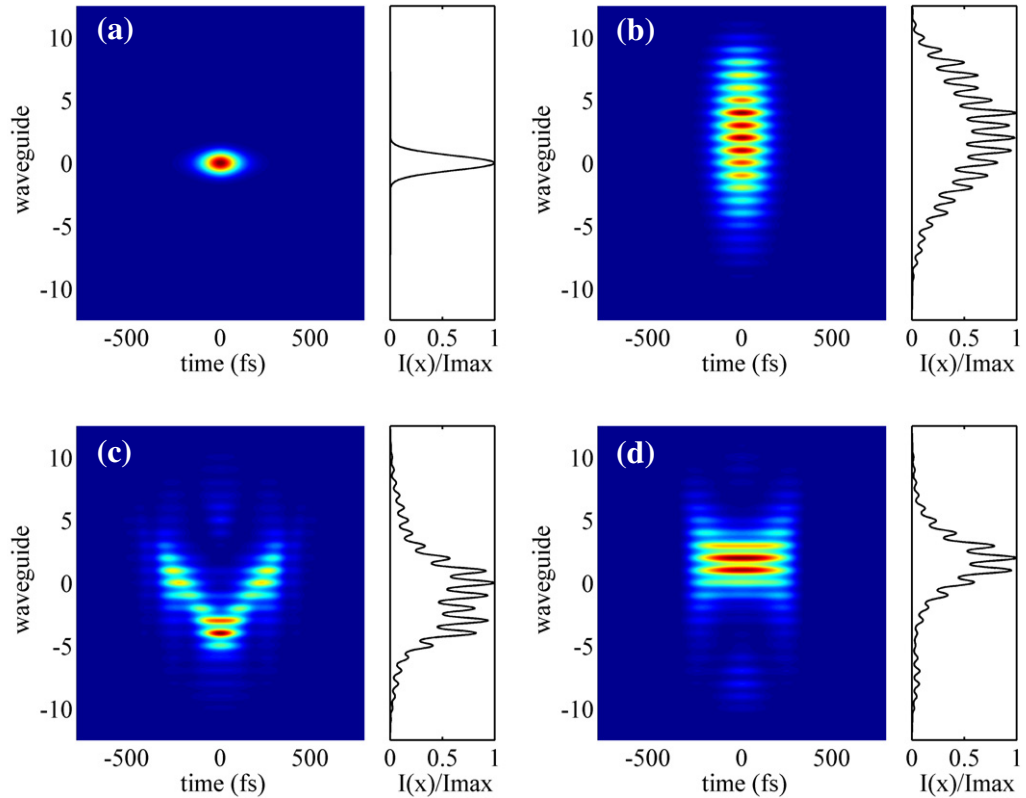


Figure 10. Spatiotemporal profile and time-integrated spatial intensity distribution (normalized) of the experimental sech-type Gaussian beam at an input angle of 4 mrad. (a) Input and (b)–(d) output profiles at $z = 5$ mm. (b) After linear propagation. (c) After nonlinear propagation at 875 W peak power in the experimental system of low 3PA ($\alpha_3 = 10^{-4} \text{ m}^{-1} \text{ W}^{-2}$). (d) After nonlinear propagation at 875 W peak power in a hypothetical system with 3PA 20 times that of the experimental system ($\alpha_3 = 20 \times 10^{-4} \text{ m}^{-1} \text{ W}^{-2}$). The respective output profile for a system without 3PA is almost identical to (c).

The input pulse depicted in figure 10(a) is given an initial tilt of 4 mrad and after 5 mm of linear propagation the output is clearly shifted, following the input tilt (see figure 10(b)). For nonlinear propagation at 875 W peak power (see figure 10(c)) the same pulse is shifted to a direction opposite to the initial after almost half a cycle of oscillation. It is evident that due to pulse broadening and discrete diffraction, pulse splitting is intense.

Although it is apparent from figure 10(c) that absorption is not necessary in this procedure, its presence can serve as an enhancing factor or even an alternative mechanism to this performance (for low normal GVD systems). To this end, and to emphasize the resemblance to the conclusions of figure 7 which concerned the CW case, in figure 10(d) we demonstrate the spatiotemporal distribution of the initial pulse, after propagating in a hypothetical system with intense 3PA (20 times that of our experiment). Again, as in the CW case, with strong absorption a linear-like pattern as in figure 7(b) is possible, as the similar propagation directions in figures 10(b) and (d) indicate. Naturally, in the presence of countable absorption, the lower the GVD coefficient, the more the time-integrated output will resemble the CW beam behavior.

The fact that directed pulse propagation at will can be implemented either with the aid of normal dispersion or absorption provides an extremely useful versatility. Depending on whether pulse shaping is a desired effect, one can have the same results (in terms of beam direction) with low GVD and countable absorption, thus not significantly altering the temporal unity of the pulse.

7. Conclusions

In this work we have showed how the interplay between discrete diffraction, Kerr nonlinearity and a mechanism that effectively weakens the nonlinear part of the beam along the propagation can result in counter-intuitive beam steering effects. The idea is based on using nonlinearity to lock optical power in a waveguide and subsequently release it with the assistance of a peak power reducing mechanism. Although such beam dynamics can be complex, if this mechanism acts within the 1st cycle of beam oscillation, the beam direction can be engineered in a predictable non-chaotic manner. Although in CW dynamics this mechanism must be some sort of absorption, in pulsed systems this role can be played by the combined action of normal dispersion and Kerr nonlinearity. In the latter case absorption, although not necessary, acts as a further or alternative beam control factor. We experimentally demonstrated the proposed idea in an AlGaAs waveguide system with intense normal GVD and low 3PA and theoretically showed that the same dynamics are feasible in similar systems that exhibit any relative kind of absorption, such as 2PA or even linear absorption.

Acknowledgments

SD, PP and KH were supported by the Research Project ANEMOS co-financed by the European Union (European Social Fund—ESF) and Greek national funds through the Operational Program ‘Education and Lifelong Learning’ of the National Strategic Reference Framework (NSRF)—Research Funding Program: Thales. Investing in knowledge society through the European Social Fund. YK was supported by the Research Project NWDCCPS implemented within the framework of the Action ‘Supporting Postdoctoral Researchers’ of the Operational Program ‘Education and Lifelong Learning’ (Action’s Beneficiary: General Secretariat for Research and Technology), and is co-financed by the European Social Fund (ESF) and the Greek State. YL, YB and YS were supported by the Crown Center for Photonics at the Weizmann Institute and by ARO grant W911NF-12-1-0567.

References

- [1] Christodoulides D N, Lederer F and Silberberg Y 2003 Discretizing light behaviour in linear and nonlinear waveguide lattices *Nature* **424** 817–23
- [2] Eisenberg H S, Silberberg Y, Morandotti R and Aitchison J S 2000 Diffraction management *Phys. Rev. Lett.* **85** 1863–6
- [3] Christodoulides D N and Joseph R I 1988 Discrete self-focusing in nonlinear arrays of coupled waveguides *Opt. Lett.* **13** 794–6
- [4] Peschel U, Pertsch T and Lederer F 1998 Optical Bloch oscillations in waveguide arrays *Opt. Lett.* **23** 1701
- [5] Pertsch T, Dannberg P, Elflein W, Bräuer A and Lederer F 1999 Optical Bloch oscillations in temperature tuned waveguide arrays *Phys. Rev. Lett.* **83** 4752–5

- [6] Pertsch T, Zentgraf T, Peschel U, Bräuer A and Lederer F 2002 Beam steering in waveguide arrays *Appl. Phys. Lett.* **80** 3247–9
- [7] Morandotti R, Peschel U, Aitchison J S, Eisenberg H S and Silberberg Y 1999 Experimental observation of linear and nonlinear optical Bloch oscillations *Phys. Rev. Lett.* **83** 4756–9
- [8] Berry M V and Balazs N L 1979 Nonspreading wave packets *Am. J. Phys.* **47** 264
- [9] El-Ganainy R, Makris K G, Miri M A, Christodoulides D N and Chen Z 2011 Discrete beam acceleration in uniform waveguide arrays *Phys. Rev. A* **84** 023842
- [10] Aceves A B, De Angelis C, Trillo S and Wabnitz S 1994 Storage and steering of self-trapped discrete solitons in nonlinear waveguide arrays *Opt. Lett.* **19** 332–4
- [11] Aceves A B, De Angelis C, Peschel T, Muschall R, Lederer F, Trillo S and Wabnitz S 1996 Discrete self-trapping, soliton interactions, and beam steering in nonlinear waveguide arrays *Phys. Rev. E* **53** 1172–89
- [12] Morandotti R, Peschel U, Aitchison J S, Eisenberg H S and Silberberg Y 1999 Dynamics of discrete solitons in optical waveguide arrays *Phys. Rev. Lett.* **83** 2726–9
- [13] Peschel U, Morandotti R, Arnold J M, Aitchison J S, Eisenberg H S, Silberberg Y, Pertsch T and Lederer F 2002 Optical discrete solitons in waveguide arrays: 2. Dynamic properties *J. Opt. Soc. Am. B* **19** 2637–44
- [14] Vicencio R A, Molina M I and Kivshar Y S 2003 Controlled switching of discrete solitons in waveguide arrays *Opt. Lett.* **28** 1942–4
- [15] Królikowski W and Kivshar Y S 1996 Soliton-based optical switching in waveguide arrays *J. Opt. Soc. Am. B* **13** 876–87
- [16] Kominis Y and Hizanidis K 2004 Continuous-wave-controlled steering of spatial solitons *J. Opt. Soc. Am. B* **21** 562–7
- [17] Akhmediev N and Ankiewicz A (ed) 2005 *Dissipative Solitons (Lecture Notes Phys.* vol 661) (Berlin: Springer)
- [18] Kominis Y, Droulias S, Papagiannis P and Hizanidis K 2012 Gain-controlled dissipative soliton routing in optical lattices *Phys. Rev. A* **85** 063801
- [19] Katz O, Lahini Y and Silberberg Y 2008 Multiple breakup of high-order spatial solitons *Opt. Lett.* **33** 2830–2
- [20] Lahini Y, Frumker E, Silberberg Y, Droulias S, Hizanidis K, Morandotti R and Christodoulides D N 2007 Discrete X-wave formation in nonlinear waveguide arrays *Phys. Rev. Lett.* **98** 023901
- [21] Kaup D J and Newell A C 1978 Solitons as particles, oscillators, and in slowly changing media: a singular perturbation theory *Proc. R. Soc. Lond. A* **361** 413–46
- [22] Kivshar Y S and Campbell D K 1993 Peierls–Nabarro potential barrier for highly localized nonlinear modes *Phys. Rev. E* **48** 3077–81